The effect of electrospun polycaprolactone scaffold morphology on human kidney epithelial cells

The effect of electrospun polycaprolactone scaffold morphology on human kidney epithelial cells

Todd P Burton, Anthony Corcoran, Anthony Callanan*

Institute for Bioengineering, School of Engineering, University of Edinburgh, Faraday Building, King's Buildings, EH9 3JL, UK.

*Corresponding author: Anthony Callanan; Email: anthony.callanan@ed.ac.uk;

Keywords: Tissue engineering, scaffold architecture, electrospinning, cryogenic, kidney, renal

1. ABSTRACT

There is a pressing need for further advancement in tissue engineering of functional organs with a view to providing a more clinically relevant model for drug development and reduce the dependence on organ donation. Polymer based scaffolds, such as polycaprolactone (PCL), have been highlighted as a potential avenue for tissue engineered kidneys, but there is little investigation down this stream. Focus within kidney tissue engineering has been on 2-dimensional cell culture and decellularised tissue. Electrospun polymer scaffolds can be created with a variety of fibre diameters and have shown a great potential in many areas. The variation in morphology of tissue engineering scaffold has been shown to effect the way cells behave and integrate. In this study we examined the cellular response to scaffold architecture of novel electrospun scaffold for kidney tissue engineering. Fibre diameters of 1.10±0.16 μm and 4.49±0.47 μm were used with 3 distinct scaffold architectures. Traditional random fibres were spun onto a mandrel rotating at 250 rpm, aligned at 1800 rpm with novel cryogenic fibres spun onto a mandrel loaded with dry ice rotating at 250 rpm. Human kidney epithelial cells were grown for 1 and 2 weeks. Fibre morphology had no effect of cell viability in scaffolds with a large fibre diameter but significant differences were seen in smaller fibres. Fibre diameter had a significant effect in aligned and cryogenic scaffold. Imaging detailed the differences in cell attachment due to scaffold differences. These results show that architecture of the scaffold has a profound effect on kidney cells; whether that is effects of fibre diameter on the cell attachment and viability or the effect of fibre arrangement on the distribution of cells and their alignment with fibres. Results demonstrate that PCL scaffolds have the capability to maintain kidney cells life and should be investigated further as a potential scaffold in kidney tissue engineering.

2. INTRODUCTION

Tissue engineering is a large multidisciplinary field using a combination of cells, materials and engineering to create functional tissues, with a huge potential for the treatment of a variety of diseases. There is a pressing need for further advancement of tissue engineered (TE) functional organs, with a view to replacing the dependency on organ donation (NHS Blood and Transplant 2015) and provide better models for drug development (Davies 2015). In 2014 alone over 5,000 people were registered on the kidney transplant list in the UK (NHS Organ Donation 2014), and in 2008/09 over 1.5 million people aged over 18 were diagnosed with chronic kidney disease, around 4% of the population (NHS Kidney care 2010).

Kidney TE is still in its infancy but has thus far predominantly focused on two-dimensional (2D) models. Murine foetal cells are the model of choice in many cases, however, these are not directly translatable to humans and would not be suitable in a clinical setting (Davies & Chang 2014; Xinaris et al. 2012; Ganeva et al. 2011). A fundamental requirement for the next translational phase is a three-dimensional (3D) structure, which could be a potential implantation treatment. This has in part been shown by the development of 3D organoids, such as ureteric buds, which utilise human induced pluripotent stem cells (iHPSC) and have given rise to a clinically relevant platform of cells (Xia et al. 2013; Takasato et al. 2014; Xia et al. 2014; Takasato et al. 2015). These have shown promise but lack the expansion and functional capabilities necessary for a TE kidney (Davies et al. 2014).

Decellularised tissue, in-situ regeneration and scaffold technologies have all been highlighted as potential routes for TE kidneys (Davies et al. 2014). Decellularised tissue is the most widely explored 3D kidney TE method, due to its physical and mechanical properties (Nakayama et al. 2010; Uzarski et al. 2014; Yu et al. 2014; He et al. 2016). Using this technique, a rat kidney model has been shown to produce urine *in vitro* and *in vivo*; however, barriers for TE kidneys still remain including optimisation of cell seeding processes, the scaling up of existing strategies, and availability of a feasible cell source (Song et al. 2013). Despite its widespread use in tissue engineering decellularised tissue has no standardized protocol, producing variations between scaffolds (He & Callanan 2013).

Polymer scaffold have been previously used to create renal units *in vivo*, this used subcutaneous implantation into a murine model of polyglycolic acid scaffolds seeded with renal segments (Kim et al. 2003). Another group has utilised natural and synthetic polymers to create an *in vitro* model of the glomerular capillary by producing a confluent monolayer of podocytes and endothelial cells (Slater et al. 2011). This model showed evidence of cell-cell communication and identified that both matrix protein and structure are important for monolayer formation.

The use of polycaprolactone (PCL) has been explored in many areas of tissue engineering using a variety of fabrication techniques (E. Sachlos and J.T. Czernuszka 2003; Woodruff & Hutmacher 2010). It is an excellent biomaterial due to its mechanical properties and biocompatibility. Tissue engineering applications include: bone (Bye et al. 2013; Phipps et al. 2012), cartilage (Steele et al. 2014), ligament (Petrigliano et al. 2014), cornea (Baradaran-Rafii et al. 2016) and vascular (Wise et al. 2011) to name a few. Polymer-based scaffolds, such as PCL, have been highlighted as a potential avenue for tissue engineered kidneys (Moon et al. 2016), but there is little investigation down this stream.

Electrospinning is a fabrication technique used in tissue engineering (TE) to produce a non-woven structure with fibre diameters from 10's of nanometers to 10's of micrometres (Huang et al. 2006; Pham et al. 2006b). This variation in morphology has been shown to affect the way cells behave and integrate with the scaffold, larger fibres allow for greater cell integration, nanofibres represent the natural ECM and aligned fibres have shown to guide neural, vascular and cornea cell growth (Yan et al. 2012; Balguid et al. 2009; Wang et al. 2012). Other methods have been proposed to increase the porosity of scaffolds to allow for greater cell integration; dual-spinning using a water soluble sacrificial material allows for a scaffold with greater porosity (Lowery et al. 2010; Phipps et al. 2012) and techniques such as cell electrospinning enable cell to be directly integrated within the scaffold (Jayasinghe 2013; Townsend-Nicholson & Jayasinghe 2006). Techniques such as cryogenic electrospinning have also been proposed, this utilises the deposition of ice crystals on a cooled surface as a template for electrospun fibres, giving greater porosity (Leong et al. 2013; Bulysheva et al. 2013).

The focus of this work is to explore the potential of polymer scaffolds for kidney TE. We will examine the cellular response of human kidney epithelial cells (RC-124) to fibre diameter and morphology of electrospun polycaprolactone scaffolds. Due to a paucity of research looking at the desired environment for kidney cells within a TE platform this study is vital to gain a better understanding of cellular response.

3. MATERIALS AND METHODS

3.1 SCAFFOLD FACRICATION

Scaffolds of two fibre diameters and 3 architecture types were created and will be referred to as: large random (LR), large aligned (LA), large cryogenic (LC), small random (SR), small aligned (SA) and small cryogenic (SC).

3.1.1 ELECTROSPINNING

Non-woven electrospun meshes were produced using an EC-DIG electrospinning platform (IME Technologies, Netherlands). All fibres were collected on a rotating mandrel covered with aluminium foil, at an ambient temperature of 23°C shown at sensor for aligned and random fibres and 20 °C for cryogenic fibres (mandrel temperature not measured, mandrel filled with dry ice at -78.5 °C), figure 1. For each scaffold 4 ml of solution was used.

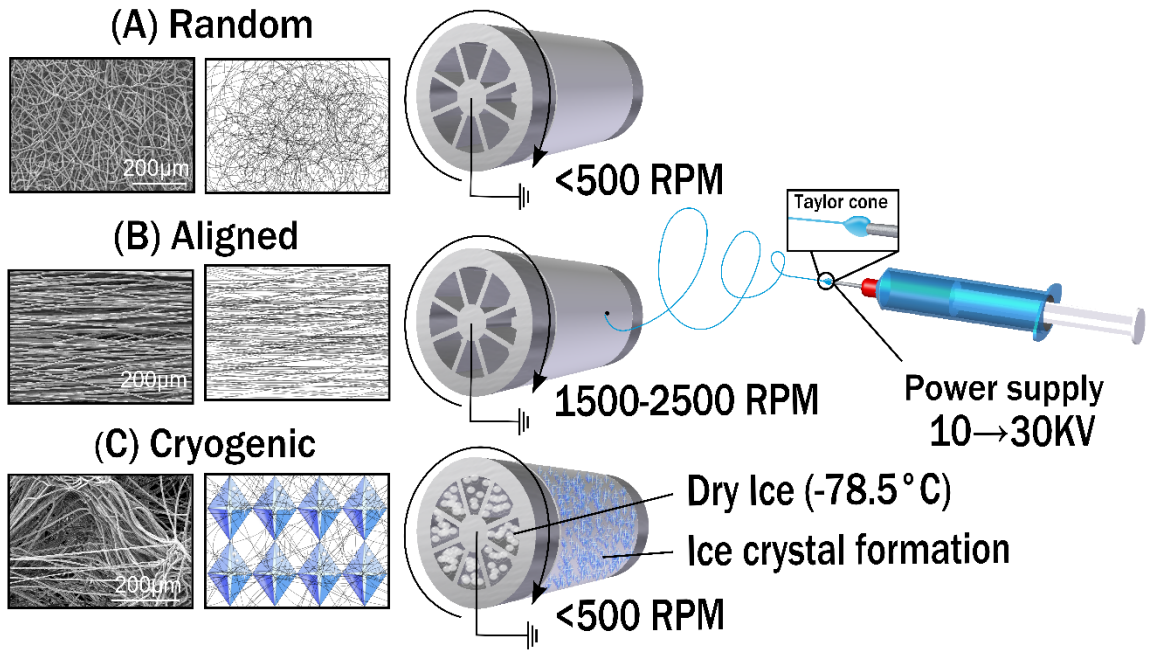

FIGURE 1: A SCHEMATIC OF THE METHODS USED TO CREATE THE DISTINCT ARCITECTURES OF ELECTROSPUN FIBRES.

Large fibres were produced by dissolving 19 % (w/v) polycaprolactone (PCL) (M_n=80,000 Da) in a 5:1 solution of chloroform and methanol, all sourced from Sigma-Aldrich, UK. A flow rate of 4 mL hr^{-1} and a 0.8mm needle was used with an accelerating voltage of +15 kV / -4 kV and a working distance of 230 mm from needle to mandrel.

Small fibres were created using a solution of 7 % (w/v) PCL in 1,1,1,3,3,3-hexafluoro-2-isopropanol (HFIP) (Manchester Organics, UK) at a flow rate of 0.8 $mlhr^{-1}$ through a needle bore of 0.4 mm and a voltage of +14 kV/ -4 kV, a working distance of 120 mm was used.

Mandrel speed was set at 250 RPM for random fibres and 1800 RPM for aligned fibres. Collected fibres were dried in a fume hood overnight, and cut into 10mm disks.

Cryogenic fibres were created by filling the mandrel with dry ice and rotating at 250 RPM, refilling every hour. The low temperature spinning causes the deposition of ice crystals on the mandrel which creates a greater space between fibres. When complete, cryogenic fibres were transferred to a freeze dryer for 24 hours and cut into 10mm disks.

3.2.2 PLASMA TREATMENT

Scaffolds were sterilised in 70 % ethanol for one hours before washing 3 times in distilled water and drying under vacuum for 24 hours prior to plasma treatment.

A Harrick Plasma cleaner and PlasmaFlo gas flow mixer (PPC-FMG-2, Harrick Plasma) was used to increase the hydrophilicity of the scaffolds for cell culture. Initial pressure was lowered to 400 mTorr before introducing O_2, pressure was stabilised at 500 mTorr and medium power (10.2 W) was applied for 30 seconds. Scaffolds were immediately submerged in PBS containing 1 % antibiotic-antimycotic (Gibco) to prevent hydrophobic recovery and transferred to a non-adherent 48 well plate with 450 µl of cell culture media.

Scaffold for water contact angle measurement was kept dry and tested immediately following treatment.

3.3 SCAFFOLD ANALYSIS

3.3.1 MECHANICAL TESTING

An Instron 3367 tensile testing machine (Instron, UK) with a 50 N load cell was used to test scaffolds to failure in tension. Samples had a gauge length of 20 mm and a width of 5 mm, with thickness measured using a digital micrometre, the strain rate was set to 50 % strain a minute. Ultimate tensile strength and incremental Young's modulus (between 0 and 10 % strain in 2 % intervals) were calculated from stress-strain graphs for each sample with $N \geq 6$ independent replicates as previously described (Callanan, Davis, T.M. McGloughlin, et al. 2014).

3.3.2 SCANNING ELECTRON MICROSCOPY

A Hitachi S4700 fuelled emission scanning electron microscope (SEM) (Hitachi) with a 5 kV accelerating voltage and a working distance of 12 mm was used to image scaffolds. Fibres were coated using an Emscope SC500A splutter coater using gold-palladium (60:40).

3.3.3 POROSITY

Estimated porosity was taken by measuring the density of scaffold and dividing it by the density of the polymer as in the equation below:

$$Porosity = \left(1 - \frac{Density\ of\ Scaffold}{Density\ of\ Polymer}\right) X\ 100$$

3.3.4 CONTACT ANGLE

A CellScale Microsquisher (CellScale, Canada) with monochrome 1280X 960 pixel camera was used to capture water contact angle with images taken at a frequency of 5 Hz. A single droplet was ejected from a P20 pipette and the droplet was recorded over 5 seconds. Images were analysed using ImageJ software and the DropSnake plugin (Stalder et al. 2006).

3.3.5 X-RAY PHOTOELECTRON SPECTROSCOPY

X-Ray photoelectron spectroscopy (XPS) spectra were taken using a VG Sigma Probe instrument (Thermo Fisher, UK) with an A1 K alpha radiation source. Full scans used a pass energy of 80 eV and a step size of 1 eV, C1 and O1 scans used a pass energy of 20eV and a step size of 0.1eV. Peak analysis was performed using Renishaw Wire2 software.

3.4 CELL CULTURE

A human kidney primary epithelial cell line (RC-124) was purchased from cell line services (CLS, Germany). Cells are from non-tumour tissue of a 63 year old male diagnosed with kidney carcinoma in 1998, cells are immortalised and monolayer adherent. Cells were expanded in McCoy's 5A media containing: antibiotic-antimycotic 1%, L-Glutamine 1% and foetal bovine serum 10% (all media and supplements from Gibco, ThermoFisher Scientific, UK). Cultures were maintained at 37°C with 5% CO_2 and media changed 2/3 times a week, Accutase was used for detaching cells from culture flask.

A suspension of 100,000 cells (Passage 17) in 50 µl of culture media was seeded to each scaffold and left to attach for 1 hour before an additional 400 µl of media was added. Scaffolds were cultured for 7 and 14 days prior to further experimentation, with media changed 3 times a week.

3.4.1 CELL VIABILITY

Cell metabolism was assessed using a CellTitre-Blue® assay (Promega, UK). Scaffold were washed 3 times in PBS and 80 µl of CellTitre-Blue® assay was added to 400 µl cell culture media (1:5) and incubated for 2 hours. Fluorescence was read using a microplate reader (Modulus II 9300-062, Turner Biosystems) at Ex 520 nm Em 580-640 nm, $N \geq 4$ independent replicates.

3.4.2 DNA QUANTIFICATION

Scaffold were freeze dried and incubated in a papain digest solution of: 2.5 units/ml papain, 5 mM cysteine HCL and 5 mM EDTA in PBS (all reagents from Sigma Aldrich, UK) at 60 °C for 48 hours and periodically mixed using a vortexer. Total DNA content of the samples was calculated using a Quant-iT™ PicoGreen® assay kit (ThermoFisher, UK) as per the manufacturers' instructions. Fluorescence was read using a microplate reader at Ex 490 nm Em 510-570 nm, $N \geq 4$ independent replicates.

3.4.3 CELL IMAGING

Scaffolds were washed 3 times in PBS and fixed using 300 µl of 3.7% (v/v) formalin solution in PBS for 10 minutes, then washed again 3 times in PBS. A 0.2% (v/v) TritonX-100 solution in PBS was used for permeabilization, with 300 µl added for 5 minutes before washing 3 times in PBS.

Cells were stained with 0.1 mg/ml 4',6-diamidino-2-phenylindole (DAPI) (Sigma-Aldrich, UK) in PBS for 10 minutes then 1 µl of 1000X Phalloidin-iFluor™ 514 conjugate (AAT Bioquest, Stratech) in 1 ml PBS with 1 % bovine serum albumin for 30 minutes. Scaffolds were washed 3 times in PBS after each stage.

Cells were imaged using a custom multi-photon microscope. This system consists of a mode-locked ND:YVO_4 laser source (PicoTrain, Spectra Physics) to generate both a Stokes pulse (6 ps, 1064 nm) and drive an optical parametric oscillator (OPO) (Levante Emerald, APE). The OPO provides a tuneable excitation pulse across 700-1000 nm allowing coherent anti- Stokes Raman scattering (CARS), second harmonic generation (SHG) and two-photon excitation fluorescence (TPEF) microscopy. The two pulse trains are coupled into an inverted microscope (Nikon BV 'C1', Amsterdam, Netherlands) and focused onto the sample with a 25 times water-immersion objective lens with an numerical aperture of 1.05 (XLPlan N, Olympus). Images from the CARS and TPEF signals were recorded on two photomultiplier tubes (R3896, Hamamatsu). The lateral and depth resolution of this objective was measured to be 0.25 and 1.1 μm, respectively (Mouras et al. 2013).

The CARS signal was generated from the asymmetrical CH_2 stretch of the scaffold at 812.5 nm (2911 cm^{-1} wavenumbers). The same OPO beam was used to excite the broad two-photon spectrum in the Phalloidin and DAPI. The signals were separated with two dichroic filter cubes at 649 nm, 570 nm, along with band pass filters with transmission peaks at 660 nm, 585 nm, 545 nm for the CARS, Phalloidin-iFluor™ and DAPI, respectively.

3.4.4 REVERSE TRANSCRIPTION REAL-TIME POLYMERASE CHAIN REACTION

Reverse transcription real-time polymerase chain reaction (RT-qPCR) was performed in a two-step process. Cells and scaffolds were homogenised using Trizol® (Life Technologies) and RNA, DNA and proteins isolated with the addition of chloroform. RNA was separated by harvesting the clear supernatant and isolated using an RNeasy kit (Qiagen) as per manufacturer's instructions. The cDNA was obtained from reverse transcription using an InProm-II kit (Promega), according to manufacturer's instructions, and a PCR machine (Applied Biosystems Proflex PCR system). Real-time quantitative polymerase chain reaction (qPCR) was carried using (LightCycler 480 11/96, Roche Diagnostics Ltd) machine and primers (Sigma Aldrich) for Glyceraldehyde-3-phosphate dehydrogenase (GAPDH) (forward: 5'-GTCTCCTCTGACTTCAACAG, reverse: 5'-GTTGTCATACCAGGAAATGAG), Cytokeratine-18 (KRT-18) (forward: 5'-

CCTGTTAGGTGTGGGTGGAT, reverse: 5'-GAGTGGAGGTGATCAGAGGG), E-Cadherin (E-Cad) (forward: 5'-AGCGTATGTGAACTCCCCAA, reverse: 5'-AGTCCTATTGCCTGCCTGTT), alanyl aminopeptidase (ANPEP) (forward: 5'-TGGCCACTACACAGATGCAG, reverse: 5'-CTGGGACCTTTGGGAAGCAT) and kidney injury molecule-1 (KIM-1) (forward: 5'-TCCGTGGCCCTTTTTGCTTA, reverse: '- GGATCAGCGTTCAGATCCAGG) by using SensiFAST™ SYBR® Hi-ROX kit (Bioline) according to manufacturer's protocol. The gene expression levels were normalised using the expression of the GAPDH housekeeping gene and were presented as a relative expression. The $2^{-\Delta\Delta Ct}$ method (Callanan, Davis, T. M. McGloughlin, et al. 2014) was used to calculate relative mRNA levels of ANPEP, AQP-2, E-Cad, KIM-1, KRT-8 and KRT-18 of scaffolds to tissue culture plastic.

3.5 STATISTICAL ANALYSIS

Before comparison using ANOVA Levene's test for equal variances was used and appropriate statistical tests were selected. Mechanical data and fibre diameter is presented as mean ± standard deviation, all other results are presented as mean ± 95 % confidence interval. A one-way Welch's ANOVA with post hoc Games-Howell for unequal variances was used to assess the differences in fibre diameter due to spinning condition as well as mechanical data and DNA quantification. CellTitre-Blue® and water contact angle analysis was performed using a one-way ANOVA with a post hoc tukey test. Comparisons of RT-qPCR for scaffolds against tissue culture plastic were made using a two-tailed student t-test with either equal or unequal variance dependant on the outcome of an f-test, statistical significance determined by $p<0.05$.

4. RESULTS

4.1 ELECTROSPUN SCAFFOLDS

Electrospinning produced scaffolds consisting of non-woven fibres, spinning at low speed produced random fibres figure 2(a, b), high speed created highly aligned fibres, figure 2 (c, d). Cryogenic

electrospinning produced scaffolds with visibly greater pores, the large diameter fibre also produced dense regions of fibres between more porous zones attributed to the attraction towards ice crystal peaks deposited on the mandrel, figure 2 (e-h). Fibre diameters were determined from SEM images showing average large and small fibre diameter and standard deviation of 4.68±0.58 µm and 1.12±0.22 µm respectively, table 1. Discrepancies were found in fiber sizes of the same percentage weight solution due to natural variation in spinning conditions $F(2, 197)=99.44$, $p=0$, diameters of LA fibres were significantly different to both LC and LR $p=0$, with all small fibre diameters presenting with significant differences to each other, $F(2, 145)=55.34$, $p=0$. Clear differences between large and small fibre diameters can be attributed to the polymer solution properties for each scaffold, as viscosity of solution is a big contributor towards fiber size (Sill & von Recum 2008; Pham et al. 2006a). These differences in fibre diameter and architecture result in stark differences in scaffold thickness with cryogenic scaffolds at 800 µm thick compared to 90-180 µm for random and aligned scaffolds, table 1.

TABLE 1: MECHANICAL AND PHYSICAL PROPERTIES OF THE ELECTROSPUN SCAFFOLDS.

		Large			Small		
		Random	**Aligned**	**Cryogenic**	**Random**	**Aligned**	**Cryogenic**
Fibre diameter, µm		4.45±0.47	5.37±0.52	4.47±0.38	1.11±0.16	0.95±0.18	1.29±0.22
Approximate scaffold thickness µm		140	180	800	120	100	800
Porosity, % $\left(1-\frac{Density\ of\ Scaffold}{Density\ of\ Polymer}\right) X\ 100$		84.9	82.5	96.8	92.6	88.6	98.4
Ultimate tensile strength, MPa		1.45±0.24	3.92±0.68	0.26±0.10	1.60±0.31	8.62±1.98	0.17±0.06
Strain at break		4.91±2.59	6.05±0.97	9.36±1.07	5.31±1.24	0.81 ±0.16	5.37±1.60
Young's Modulus at % Strain, MPa	**0-2**	8.41±1.62	36.10±4.25	0.24±0.08	3.61±0.79	18.37±3.86	0.12±0.06
	2-4	8.01±0.74	29.76±2.37	0.27±0.08	3.57±0.78	27.17±4.35	0.15±0.07
	4-6	6.61±0.5	22.73±1.97	0.27±0.7	3.25±0.63	29.92±3.54	0.17±0.06
	6-8	5.25±0.55	16.28±1.99	0.26±0.10	2.91±0.54	26.56±2.71	0.17±0.05
	8-10	4.07±0.73	9.99±1.71	0.23±0.05	2.54±0.59	21.94±2.29	0.17±0.04

	0-10	6.58±0.51	23.05±1.99	0.26±0.07	3.21±0.63	26.66±3.0	0.16±0.05
Water contact angle (1 second)	**Not plasma treated**	106.4±3.1°	104.1±7.6°	118.3±9.1°	98.4±27.3°	88.4±7.2°	105.5±9.0°
	Plasma Treated	0	1.1±2.25°	75.1±39.3°	22.3±2.8°	11.3±13.1°	68.1±52.8°

Differences can be seen in the mechanical properties of each scaffold due to both fibre diameter and scaffold architecture. Significant differences were found in both the UTS $F(5, 18)=134.8$, $p=0$ and Young's modulus $F(5, 17)=555.65$, $p=0$ of different architectures for both small and large fibres. Post hoc tests indicated the effect of fibre diameter on tensile Young's modulus at 0-10% strain was significantly different in random fibres $p=0$, but no significant differences were found in aligned or cryogenic. Only aligned fibres demonstrated significant differences in UTS due to fibre diameter, $P=0.004$, table 1. There were no differences found in the mechanical properties of plasma treated and non-plasma treated fibres (supplementary data).

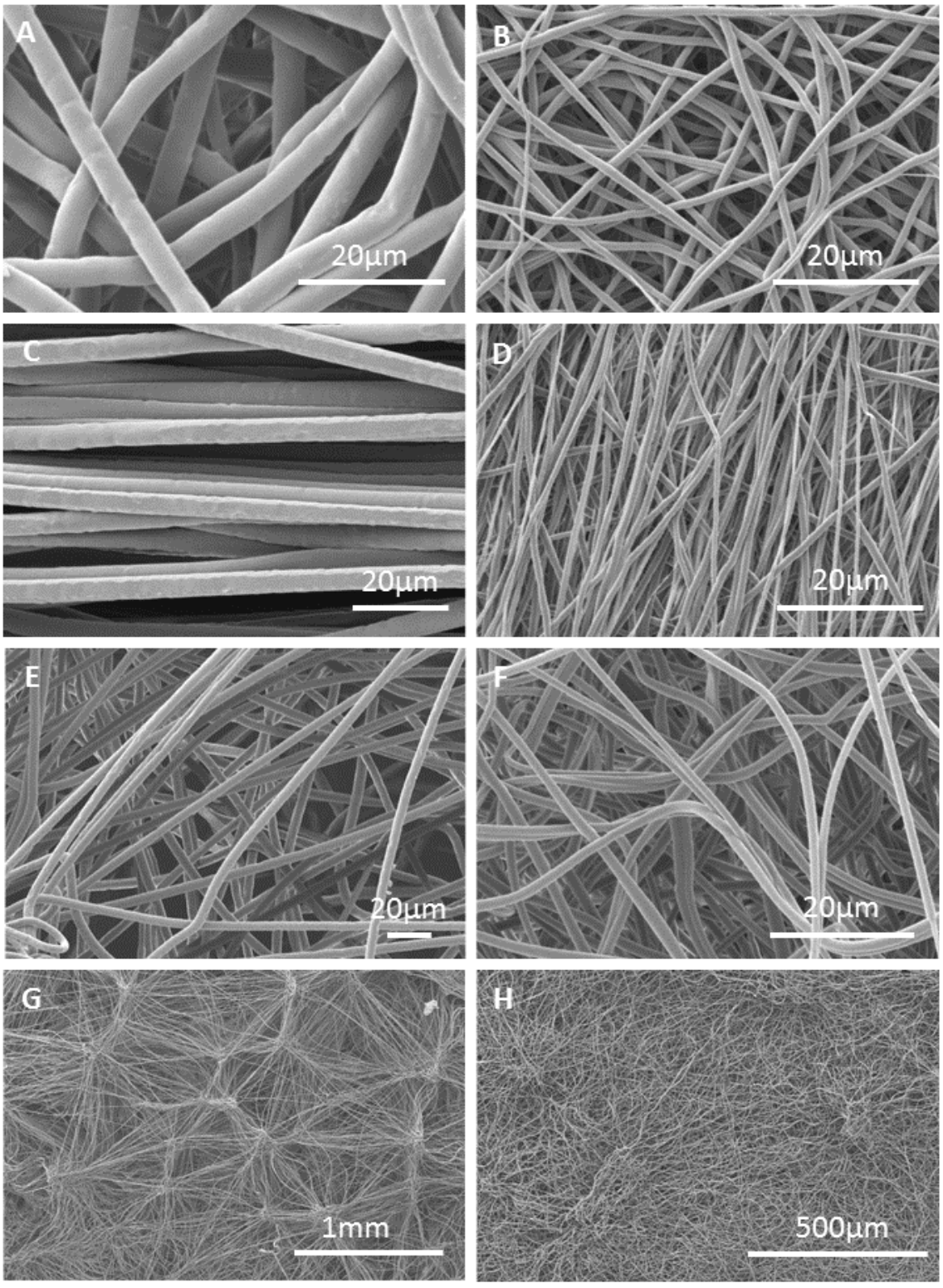

FIGURE 2: SEM OF ELECTROSPUN FIBRES SHOWING THE DIFFERENCES OF SCAFFOLD ARCHITECTURE, (A) LARGE RANDOM, (B) SMALL RANDOM, (C) LARGE ALIGNED, (D) SMALL ALIGNED, (E, G) LARGE CRYOGENIC AND (F, H) SMALL CRYOGENIC.

4.2 PLASMA TREATMENT

Plasma treatment was successful in reducing the hydrophobicity of the scaffold, a comparison of water contact angle for cast films created using 17 % w/v PCL in chloroform/ methanol (5:1) and 7 % w/v PCL in HFIP solutions presented with significant differences between plasma 53.1±6.2 ° and non-plasma treatment 76.2±3.4° $F(3, 24)=44$, $p=0$, no differences were seen as a result of the solvent used, table 1. It can be seen that plasma treatment resulted in a significant reduction in water contact angle in all samples, table 1. The water contact angle of electrospun scaffold is somewhat higher than the film counterpart which can be attributed to an increase in surface roughness (Yuan & Lee 2013). Water absorption by both random and aligned scaffolds was instantaneous, cryogenic scaffolds took on average 12 seconds to full absorb the water droplet.

X-Ray photoelectron spectroscopy confirmed that there was a distinct increase in the atomic percentage of oxygen (O) present after plasma treatment. Average O in plasma treated and non-plasma treated scaffolds was 26.0±1.5 % and 21.7±0.7 % respectively, and average carbon present (C) in plasma treated and non-plasma treated scaffolds was 74.0±1.5% and 78.4±0.7 % respectively. This increase in surface oxygen is a direct result of surface oxidation due to O_2 plasma treatment (Martins et al. 2009; Jordá-Vilaplana et al. 2014). Issues arose due to scaffold porosity that prevented attaining measurements for plasma treated SC, table 2.

TABLE 2 : ELEMENT COMPOSITION, DETERMINED BY XPS, OF SCAFFOLD BEFORE AND AFTER PLASMA TREATMENT, CARBON (C), OXYGEN (O)

		Large			**Small**		
		Random	**Aligned**	**Cryogenic**	**Random**	**Aligned**	**Cryogenic**
Not Plasma Treated	C %	77.3	79.3	78.4	78.1	78.8	78.5
	O %	22.7	20.8	21.6	21.9	21.1	21.6
Plasma treated	C %	75.3	75.1	71.6	74.2	73.7	-
	O %	24.7	24.9	28.4	25.8	26.3	-

4.2 CELL VILABILITY

The viability of cells, assessed by CellTitre blue assay, showed significant differences after 7 days ($F(5, 24)=9$, $p<0.001$) and 14 days ($F(5, 24)=17$, $P<0.001$). Variations were seen between fibre diameters at 7 days for aligned ($p=0.043$) and cryogenic ($p=0.044$), and at 14 days for cryogenic ($p<0.001$). Significance differences between architecture was seen at 7 days for SR/SC ($p=0.0025$), and at 14 days for SA/SC ($p<0.001$) and SR/SC ($p<0.001$). The architecture of large fibres appeared to have no statistically significant effect on cell viability at 7 or 14 days. Although cell viability increased from 7 to 14 days in all cases except SC (Figure 3) the increase was not statistically significant for any group, this may be as a result of the relatively high seeding density. It is worth reiterating that scaffold were cut into 10 mm disks and thus cells were probably reaching confluency on scaffolds with any further expansion penetrating into the scaffolds.

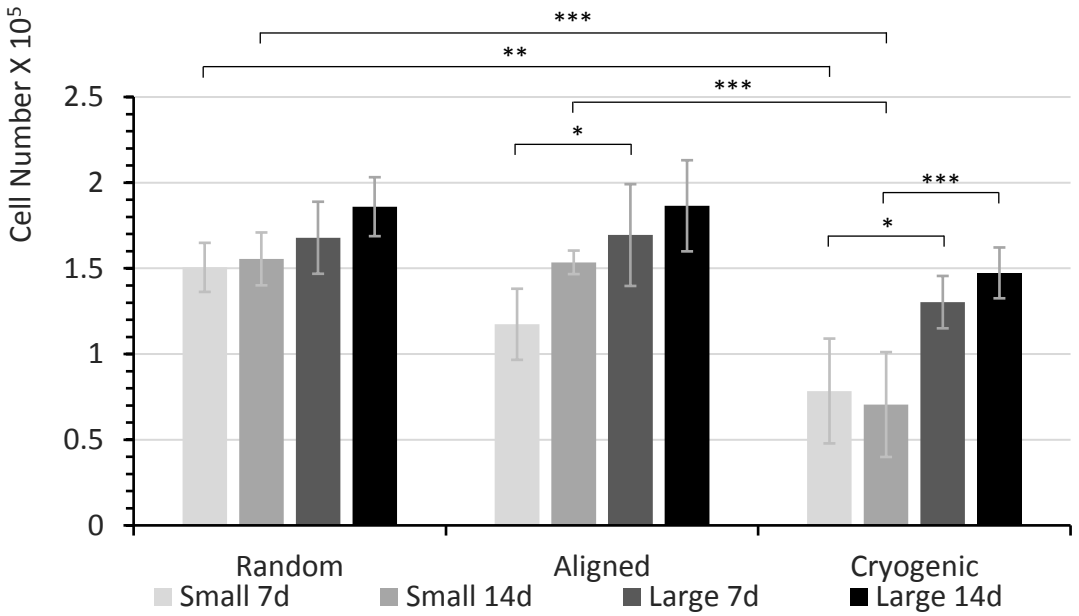

FIGURE 3: CELL ATTACHMENT AND VIABILITY OF RC-124 CELLS AT 7 AND 14 DAYS ON RANDOM, ALIGNED AND CRYOGENIC SCAFFOLDS OF TWO DIFFERENT FIBRE DIAMETERS. FLUORESCENCE VALUES HAVE BEEN NORMALISED TO A WELL CONTAINING 100,000 CELLS. DATA PRESENTED AS MEAN ± 95 % CONFIDENCE INTERVAL, STATISTICS PERFORMED ONE WAY ANOVA USING A POST HOC TUKEY TEST, N=5, * P<0.05, **P<0.01 AND *** P<0.001

4.3 DNA QUANTIFICATION

DNA quantity increased between 7 and 14 days in all cases, figure 4. A comparison of the DNA quantity in different scaffold architectures showed significances at 7 days $F(5, 11)=18$, $p=0$, specifically: SR/SC ($p=0.017$) and LR/LC ($p=0.024$) and at 14 days $F(5, 10)=12$, $p=0.001$, specifically: SA/SC ($p=0.002$). Significant differences in DNA quantity due to fibre diameter were found in random ($p=0$), and cryogenic fibres ($p=0.014$), at 7 days, no significant differences were found after 14 days. The results reflect similarly the results produced using CellTitre blue assay with a greater number of cell present on scaffolds with a larger fibre diameter (Figure 3 and 4).

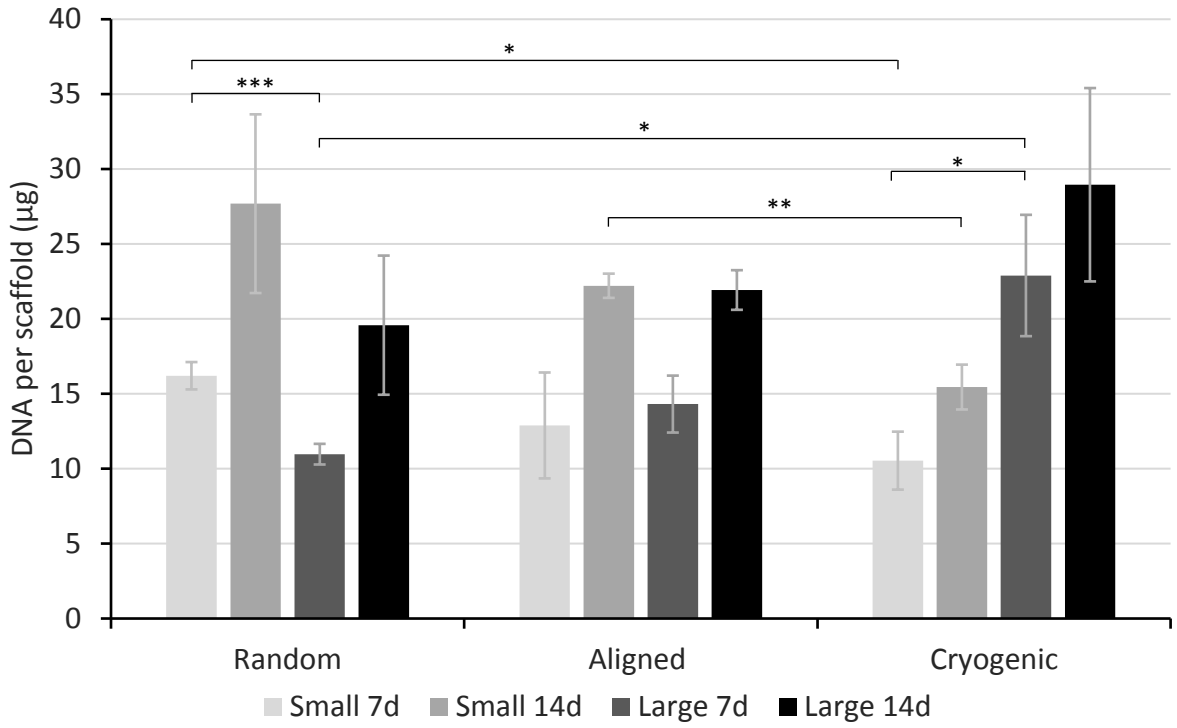

FIGURE 4: PICOGREEN ASSAY AT 7 AND 14 DAYS SHOWING THE DNA QUANTITY PER SCAFFOLDS. DATA IS PRESENTED AS MEAN ± 95 % CONFIDENCE INTERVAL, STATISTICS PERFORMED WITH A ONE-WAY ANOVA USING A POST-HOC GAMES-HOWEL TEST DUE TO UNEQUAL VARIANCES, N=5, * P<0.05, ** P<0.01 AND *** P<0.001.

4.4 CELL IMAGING

Images taken using CARS and TPEF compounded results gained by DNA quantification and CellTitre blue, cell seeded to random scaffolds are seen to be high in numbers and spread between fibres, figure 5 (a, b). Aligned fibres have a high number of cells and appear to be in a highly linear orientation on large fibres, due to a greater uniformity of fibre direction, figure 5(c); the smaller fibre scaffolds did not, to the same extent, result in the linear organisation of cells along the fibre, figure 5 (d). The porosity of the cryogenic scaffolds can be seen in figure 5(e, f), cells have aligned along fibres due to the distance between adjacent fibres. Cells could be seen throughout a 200 µm z-stack image of the cryogenic scaffold (data not shown), using the CARS and TPEF microscope, greater than the thickness of both the random and aligned scaffolds, scattering and signal loss prevented imaging any deeper into the samples.

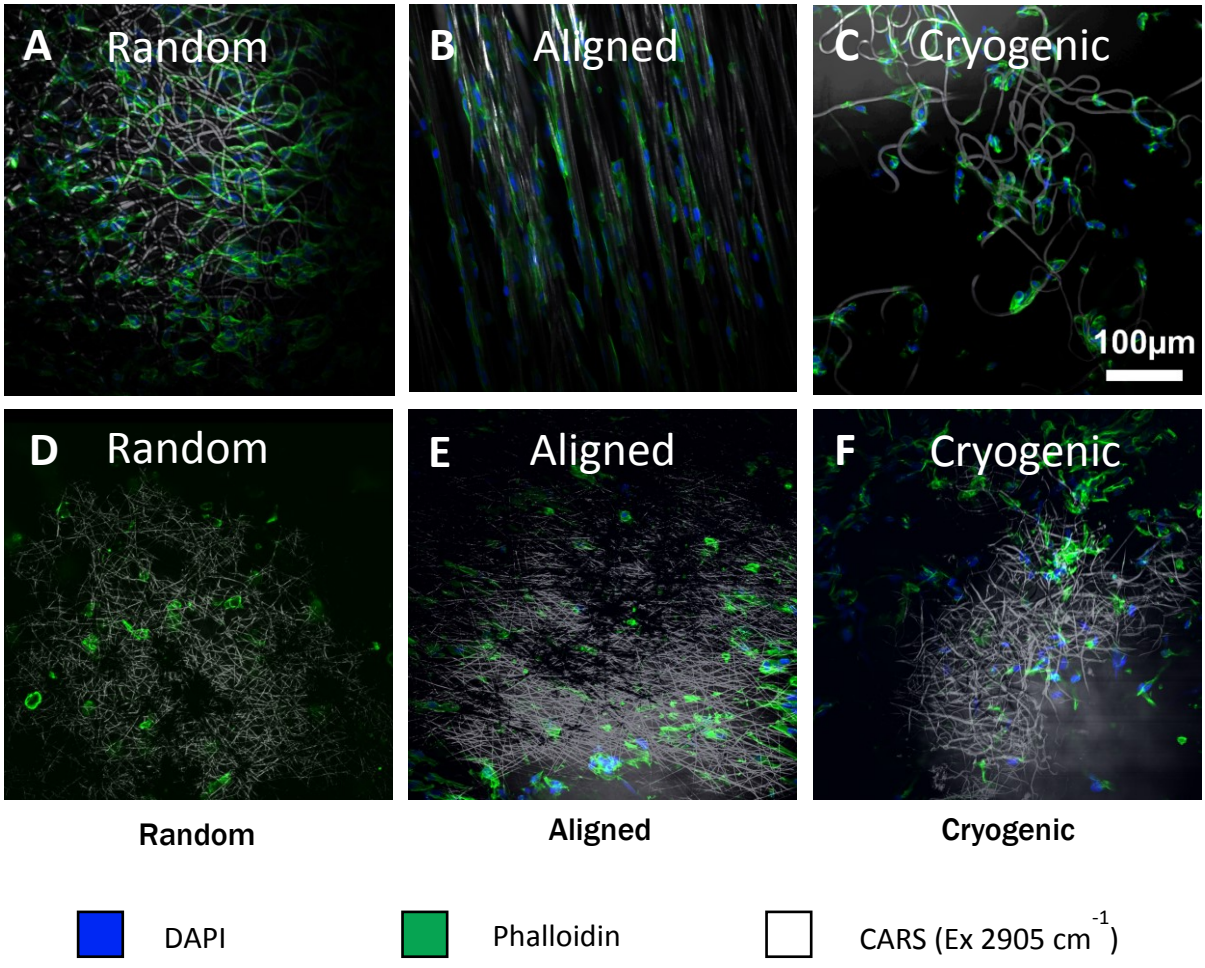

Figure 5: Two-photon excitation fluorescence (TPEF) and coherent anti-stokes Rahman scattering (CARS) images of RC-124 cells on scaffolds at 7 days (a) LR, (b) LA, (C) LC, (d) SR, (e)

SA and (f) SC. Green highlights the actin filaments, blue shows the cell nucleus and white is the PCL scaffold; clearly showing the impact of the scaffold architecture on cells growth.

4.5 GENE ANALYSIS

The RT-qPCR performed used the DDCt method showing gene expression relative of cell GAPDH to cells grown on tissue culture plastic. This showed a significant increase of relative expression of ANPEP for all large scaffolds at both 7 days (LR p=0.0019, LA p=0.012, LC p=0.032) and 14 days (LR p=0.0066, LA p=0.0028, LC p=0.038), but only showed a significant increase for small fibres on random (p=0.0037) and cryogenic (p=0.040) scaffolds at 7 days. Relative expression of E-Cad was decreased at 7 days on small and large aligned (p=0.0050 and p=0.045 respectively) scaffolds and small cryogenic (p=0.041), at 14 days large aligned (p=0.042) scaffolds showed a significant increase in E-Cad expression. KIM-1 expression only showed significant decreases at 7 days in small aligned and cryogenic scaffolds (p=0.036 and p=0.012 respectively), at 14 days only small cryogenic scaffolds (p=0.035) showed a significant difference compared to tissue culture plastic. There were no significant differences in the expression of KRT-18 (Figure 6).

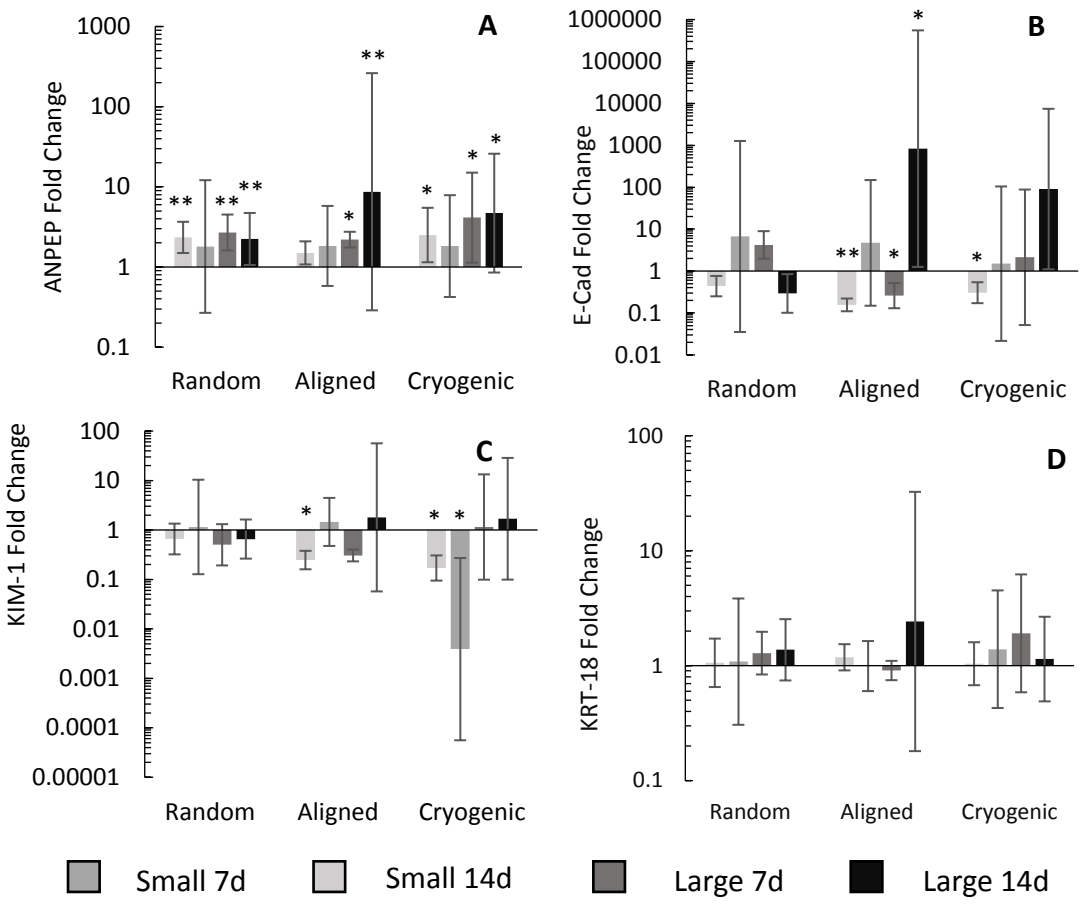

FIGURE 6: RT-QPCR DATA PRESENTED USING THE 2^{-DDCT} METHOD SHOWING THE EXPRESSION RELATIVE TO GAPDH OF 4 GENES: (A)ANPEP, (B) E-CAD, (C) KIM-1 AND (D) KRT-18 TO GAPDH, COMPARED TO CELLS GROWN ON TISSUE CULTURE PLASTIC. DATA SHOWN AS MEAN ± 95 % CONFIDENCE INTERVAL WITH STATISTICS PERFORMED USING A STUDENTS T-TEST WITH EQUAL OR UNEQUAL VARIANCES, DEPENDING ON THE OUTCOME OF AN F-TEST. *P<0.05, **P<0.01.

5. DISCUSSION

Current research in kidney tissue engineering predominantly focuses on 2D cell culture (Xia et al. 2013; Takasato et al. 2015; Takasato et al. 2014; Taguchi et al. 2014) and decellularised tissue (Peloso et al. 2016; Song et al. 2013). Decellularised tissue is favourable due to its physical and chemical characteristics that support cells and control cell physiology (Peloso et al. 2016); however, cells produce their own ECM and synthetic scaffolds can provide a foundation to build upon (O'Brien

2011). These synthetic scaffolds are scaled more easily, can be highly controlled and modified, as well as offering better safety and repeatability (Dhandayuthapani et al. 2011; Saha et al. 2007).

Muscular skeletal as well as vascular and skin tissue engineering have dominated the focus of polymer scaffolds, but there is huge scope for their use in the development of tissue engineered complex organs. The use of synthetic matrices has been highlighted for use in organoid culture previously, specifically hydrogels (Schutgens et al. 2016), however, electrospun polymer scaffolds have also been used with renal cells (Slater et al. 2011; Kim et al. 2003). These experiments using electrospun scaffolds did not consider the mechanical or physical properties of the scaffolds and the effect this has on the cells. It is well documented that changes is fibre diameter and orientation induce a response of the cells in many tissue types (Yan et al. 2012; Balguid et al. 2009; Wang et al. 2012), but the effect on renal cells has been ignored until now. The diameter of the fibre determines the pore size of the scaffold, and this determines how well cells will penetrate into a scaffold (Balguid et al. 2009; Baker et al. 2008; Ju et al. 2010). Techniques such as cryogenic electrospinning have shown to create structures with a much greater porosity, enabling cell infiltration throughout the scaffold (Leong et al. 2013; Bulysheva et al. 2013; Leong et al. 2009); this can be controlled by modifying the humidity of the spinning environment, changing the amount of ice crystal formation on the cooled mandrel (Leong et al. 2013). It is essential in the culture of a complex 3D system for a distribution of cells throughout the scaffold, increasing the porosity within electrospun scaffolds by cryogenic electrospinning allows for this greater cell distribution.

The results from our mechanical testing show the breadth of physical properties that can be obtained by electrospinning. The difference seen in Young's modulus due to fibre diameter is similar to that seen in previously published work (Wong et al. 2008; Simonet et al. 2007). In our experiments LA scaffolds have a Young's modulus around 90-fold larger than large cryogenic scaffolds, small fibres in the same case presented with a 160-fold change, table 1. Interestingly, LA fibres give a larger Young's modulus in the first 4% strain before a decline of around 3 MPa for every 2% strain compared to SA counterparts; initial lower values at 0-2% strain could be partly explained in the fact that SA fibres appear to be less uniform than LA. This mechanical strength does come at the cost of

porosity. Cryogenic scaffolds have a much greater porosity and a Young's modulus have much less variance between 0-10% strain when compared to random and aligned scaffolds. To get the optimal combination of porosity and mechanical strength hybrid scaffolds can be created to form a construct with the most desirable properties (McCullen et al. 2012).

Our results regarding the use of plasma treatment to increase the hydrophilicity of polymer scaffolds largely correlates with previous studies (Martins et al. 2009; Yan et al. 2013; Suntornnond et al. 2016; Ghobeira et al. 2017), showing an altered surface chemistry whilst retaining the same mechanical properties. This results in a dramatic increase in the hydrophilicity, as demonstrated through water contact angle tests. Surface roughness is known to increase the water contact angle of materials, and the increased surface roughness of cryogenic scaffolds resulted in a delayed absorption of water (Yuan & Lee 2013).

We looked at how these different scaffold architectures effect the viability and attachment of kidney cells. As dictated in previous studies on neural and vascular cells (Daud et al. 2012; Wang et al. 2012; Christopherson et al. 2009), fibre diameter does affect the viability of cells. Similarly to our results Christopherson et al. (2009) and Daud et al. (2012) found that when fibre diameter is around 1-1.5 μm cells have a lower proliferative capacity. Although, in the Christophereon et al. study the comparison is to nanofibres, our study, similarly to Daud et al. demonstrated a comparable result with respect to larger fibres, which may be down to points of attachment. Where there are nanofibers cells have several points of attachment and can spread themselves between fibres, as fibres diameter increases so does pore size; at larger fibre diameter cells can wrap around individual fibres for attachment, there may be a critical point at around 1 μm where cells cannot determine whether to spread between fibres or attach along individual ones, this response will obviously vary depending on the size of the cell itself. Our results showed that kidney epithelial cells have a preferential for larger fibre diameter, further investigation would be necessary to determine whether a nanofibre would be preferential, although this would give rise to a decrease in cell infiltration which would be undesirable for 3D cell culture.

Despite a lower number of viable cells on LC compared to LR and LA scaffolds the difference was not a significant. This was not that case with small scaffolds where both SR and SA scaffolds had a significantly higher cell viability. The lower number of viable cells on cryogenic scaffold may be attributed to poor seeding efficiency, this is corroborated with the DNA quantification results where the DNA quantity, particularly in LC at 7 days is significantly higher compared to other scaffold types suggesting cells that fail to attach become entrapped. The DNA data follows similar trends to the cell viability data but it does highlight that cells may be dying between 7 and 14 days as DNA quantity has a greater relative increase than cell viability, this is particularity the case for the SC scaffold as cell viability decreased slightly yet DNA quantity increased. It should also be noted that the RC-124 cell line used was monolayer adherent which could affect the proliferative capacity, especially with regards to the cryogenic scaffold.

We have seen distinct morphological differences in cells grown on different architectures, similar to other findings (Yan et al. 2012; Mahjour et al. 2016; Huang et al. 2016). Our random scaffolds show cells in a more rounded morphology, spread between numerous fibres. Alignment of cells is clearly seen in large fibres with cells spread along fibres, this is not as clearly seen in smaller fibres which could be partly due to fibres being less uniformly aligned. Cell organisation on cryogenic scaffold acted similarly to aligned scaffolds in that cells attached themselves along individual fibres. These results are analogous to those presented by Huang et al. (2016) who showed an increased interaction of cells with PVA-gelatin scaffolds compared to PVA alone where spreading of cells suggests good adhesion between ECM proteins and scaffold. This cell spreading on plasma treated electrospun PCL scaffolds is beneficial to groups studying the effect of external mechanical stimulus on cells, especially in the case of aligned scaffolds. As previously mentioned fibre diameter dictates pore size and thus cell penetration into the scaffold. We were able to visualise cell penetration through a 200 μm z-stack in LC scaffolds, a depth that is thicker than both LR and LA scaffolds. Balguid et al. (2009) have shown that the larger the fibre diameter the more even the distribution of cells throughout the scaffold. To this we can add that if porosity is increased by other means, such as cryogenic electrospinning, then cell can be better distributed. This is fundamental to 3D organoid culture, if

researchers are to engineer complex organs cells need to be distributed throughout a scaffold. The issue of cell distribution has been raised with the use of decellularised tissue, getting cells to the correct site and the sheer number of cells needed is problematic (Remuzzi et al. 2017; Song et al. 2013). Polymer scaffold could be used as a conveyor for kidney cells, providing the mechanical stability and favourable environment whilst allowing cells to use their innate reorganisation potential to create kidney precursors (Davies 2015; Davies & Chang 2014; Ganeva et al. 2011; Takasato et al. 2014).

Fibre diameter has shown to affect the gene expression of cells (Hodgkinson et al. 2014; Wang et al. 2014; Bean & Tuan 2015), and cryogenic scaffolds have shown to effect the behaviour of scaffolds and give a better representation on an in vivo environment for drug development (Bulysheva et al. 2013). We found that small diameter fibres at 7 days had a significant reduction in KIM-1 expression compared to tissue culture plastic in both aligned and cryogenic scaffolds, possibly indicating healthier cells (Waanders et al. 2010). There were no significant increases in KIM-1 in any fibre diameter, and no significant differences in expression of KRT-18 showing normal gene expression for cells. There was no significant decrease of E-Cad expression after 14 days showing normal function of cells, a significant decrease in E-Cad expression has been attributed to be an indication of kidney tumour cells (Straube et al. 2011). ANPEP is a key marker for proximal tubular epithelial cells and an upregulation was seem in SR and SC scaffold at 7 days but not at 14. Interestingly, ANPEP expression at 7 and 14 days in all large scaffold was significantly different from cells grown on tissue culture plastic. This may be of some concern as ANPEP is associated with human solid tumours (Fontijn et al. 2006); however, it should be noted that the 95% confidence intervals of fold expression, in all cases except LR and LA at 7 days, is in the range of tissue culture plastic.

Our focus on singular morphologies is an initial starting point in the investigation of scaffolds for kidney tissue engineering. Notably it has been shown that hybrid scaffolds have the potential to compound the benefits of different architectures, such as utilising the mechanical properties of aligned scaffolds with the increased porosity or larger random or cryogenic fibres (Pu et al. 2014). The growth and maintenance of RC-124 cells shows that electrospun scaffolds can support kidney cell life, but

cell viability on random and aligned scaffolds can only be loosely compared to cryogenic scaffolds due to the monolayer adherent nature of the cells. These finding highlight the potential of electrospun scaffolds and justify the need to investigate the response of primary or multipotent cells grown on singular or hybrid morphologies.

Another important factor to consider is the scaffold chemistry which has a profound effect on cellular response (Saha et al. 2007; Kharaziha et al. 2013; Shah et al. 2014; Collins & Birkinshaw 2013). While we have shown the ability of plasma treated polymer electrospun scaffolds to support kidney cell life further investigation is needed to determine optimal surface chemistry to enhance cell response; this could be done using high throughput systems such as the microarray technique (Khan et al. 2010).

6. CONCLUSION

Our work shows the ability of electrospun scaffolds to host kidney cell life. Larger fibre scaffolds better support kidney cells compared with scaffolds of around 1μm, these larger fibres also allow for greater cell integration due to a greater porosity. Techniques such as cryogenic electrospinning can increase porosity further, allowing for better cell integration, and could be used as part of a hybrid scaffold to obtain optimal scaffold properties. Our work gives justification to explore the use of electrospun scaffolds within kidney tissue engineering to support primary or pluripotent cell life.

7. ACKNOWLEDGMENTS

This research is funded by an Engineering and Physical Sciences Research Council (EPSRC) Doctoral Training Partnership (DTP) Studentship. We would like the thank Prof. Alistair Elfick for use of the lab facility, Dr. Andy Downes and the Bioimaging facility in the School of engineering (Accessible via:edin.ac/1HjvbJf), for help in acquiring TPEF and CARS images and Stephen Mitchell at the BioSEM facility.

8. REFERENCES

Baker, B.M. et al., 2008. The potential to improve cell infiltration in composite fiber-aligned electrospun scaffolds by the selective removal of sacrificial fibers. *Biomaterials*, 29, pp.2348–2358.

Balguid, A. et al., 2009. Tailoring Fiber Diameter in Electrospun Poly(e-Caprolactone) Scaffolds for Optimal Cellular Infiltration in Cardiovascular Tissue Engineering. *Tissue Engineering: Part A*, 15(2), pp.437–444.

Baradaran-Rafii, A., Biazar, E. & Heidari-keshel, S., 2016. Cellular Response of Limbal Stem Cells on Polycaprolactone Nanofibrous Scaffolds for Ocular Epithelial Regeneration. *Current eye research*, 41(3), pp.326–33. Available at: http://www.ncbi.nlm.nih.gov/pubmed/25897888 [Accessed July 22, 2016].

Bean, A.C. & Tuan, R.S., 2015. Fiber diameter and seeding density influence chondrogenic differentiation of mesenchymal stem cells seeded on electrospun poly(ε-caprolactone) scaffolds. *Biomedical Materials*, 10, p.15018. Available at: http://stacks.iop.org/1748-605X/10/i=1/a=015018?key=crossref.3f2e39a99fabd0169c3336984d57041c.

Bulysheva, A.A. et al., 2013. Enhanced chemoresistance of squamous carcinoma cells grown in 3D cryogenic electrospun scaffolds. *Biomedical Materials*, 8(5), p.55009. Available at: http://stacks.iop.org/1748-605X/8/i=5/a=055009?key=crossref.b412b57aaef7ffa24172025489612a52 [Accessed July 29, 2016].

Bye, F.J. et al., 2013. Development of bilayer and trilayer nanofibrous/microfibrous scaffolds for regenerative medicine. *Biomaterials Science*, 1(9), p.942. Available at: http://xlink.rsc.org/?DOI=c3bm60074b [Accessed October 17, 2014].

Callanan, A., Davis, N.F., McGloughlin, T.M., et al., 2014. Development of a rotational cell-seeding

system for tubularized extracellular matrix (ECM) scaffolds in vascular surgery. *Journal of Biomedical Materials Research Part B: Applied Biomaterials*, 102(4), pp.781–788. Available at: http://www.ncbi.nlm.nih.gov/pubmed/24155222 [Accessed March 30, 2017].

Callanan, A., Davis, N.F., McGloughlin, T.M., et al., 2014. The effects of stent interaction on porcine urinary bladder matrix employed as stent-graft materials. *Journal of Biomechanics*, 47(8), pp.1885–1893. Available at: http://www.sciencedirect.com/science/article/pii/S0021929014001511 [Accessed March 30, 2017].

Christopherson, G.T., Song, H. & Mao, H.-Q., 2009. The influence of fiber diameter of electrospun substrates on neural stem cell differentiation and proliferation. *Biomaterials*, 30(4), pp.556–64. Available at: http://www.sciencedirect.com/science/article/pii/S0142961208007783 [Accessed December 18, 2014].

Collins, M.N. & Birkinshaw, C., 2013. Hyaluronic acid based scaffolds for tissue engineering—A review. *Carbohydrate Polymers*, 92(2), pp.1262–1279.

Daud, M.F.B. et al., 2012. An aligned 3D neuronal-glial co-culture model for peripheral nerve studies. *Biomaterials*, 33(25), pp.5901–13. Available at: http://www.sciencedirect.com/science/article/pii/S014296121200525X [Accessed November 4, 2014].

Davies, J., 2015. Self-organized Kidney Rudiments: Prospects for Better in vitro Nephrotoxicity Assays. *Biomarker Insights*, 10(S1), pp.117–123. Available at: http://www.la-press.com/self-organized-kidney-rudiments-prospects-for-better-in-vitro-nephroto-article-a4948 [Accessed October 13, 2016].

Davies, J.A. et al., 2014. Engineered kidneys: principles, progress, and prospects. *Advances in Regenerative Biology*, 1, p.24990. Available at: http://www.regenerativebiology.net/index.php/arb/article/view/24990/35885.

Davies, J.A. & Chang, C.-H., 2014. Engineering kidneys from simple cell suspensions: an exercise in self-organization. *Pediatric nephrology (Berlin, Germany)*, 29(4), pp.519–24. Available at: http://www.pubmedcentral.nih.gov/articlerender.fcgi?artid=3928531&tool=pmcentrez&rendertype=abstract [Accessed October 2, 2014].

Dhandayuthapani, B. et al., 2011. Polymeric Scaffolds in Tissue Engineering Application: A Review. *International Journal of Polymer Science*, 2011, pp.1–19. Available at: http://www.hindawi.com/journals/ijps/2011/290602/ [Accessed July 27, 2016].

E. Sachlos and J.T. Czernuszka, 2003. Making tissue engineering scaffolds work. Review on the application of solid freeform fabrication technology to the production of tissue engineering scaffolds. *European Cells and Materials*, 5, pp.29–40.

Fontijn, D. et al., 2006. CD13/Aminopeptidase N overexpression by basic fibroblast growth factor mediates enhanced invasiveness of 1F6 human melanoma cells. *British journal of cancer*, 94(11), pp.1627–36. Available at: http://www.ncbi.nlm.nih.gov/pubmed/16685268 [Accessed May 1, 2017].

Ganeva, V., Unbekandt, M. & Davies, J.A., 2011. An improved kidney dissociation and reaggregation culture system results in nephrons arranged organotypically around a single collecting duct system. *Organogenesis*, 7(2), pp.83–7. Available at: http://www.pubmedcentral.nih.gov/articlerender.fcgi?artid=3142442&tool=pmcentrez&rendertype=abstract [Accessed August 27, 2015].

Ghobeira, R. et al., 2017. Effects of different sterilization methods on the physico-chemical and bioresponsive properties of plasma-treated polycaprolactone films. *Biomedical Materials*, 12(1), p.15017. Available at: http://stacks.iop.org/1748-605X/12/i=1/a=015017?key=crossref.13e380618b57fadb002caa52849eba1f [Accessed April 20, 2017].

He, M. et al., 2016. Optimization of SDS exposure on preservation of ECM characteristics in whole

organ decellularization of rat kidneys. *Journal of Biomedical Materials Research - Part B Applied Biomaterials*, pp.1–9.

He, M. & Callanan, A., 2013. Comparison of methods for whole-organ decellularization in tissue engineering of bioartificial organs. *Tissue engineering. Part B, Reviews*, 19(3), pp.194–208. Available at: http://www.pubmedcentral.nih.gov/articlerender.fcgi?artid=3627431&tool=pmcentrez&rendertype=abstract [Accessed November 12, 2014].

Hodgkinson, T., Yuan, X.-F. & Bayat, A., 2014. Electrospun silk fibroin fiber diameter influences in vitro dermal fibroblast behavior and promotes healing of ex vivo wound models. *Journal of Tissue Engineering*, 5, pp.1–13. Available at: http://tej.sagepub.com/lookup/doi/10.1177/2041731414551661 [Accessed July 29, 2016].

Huang, C. et al., 2006. Electrospun polymer nanofibres with small diameters. *Nanotechnology*, 17(6), pp.1558–1563. Available at: http://stacks.iop.org/0957-4484/17/i=6/a=004?key=crossref.4ea2f4bc197bf14317fd9df4526c10ba [Accessed November 26, 2014].

Huang, C.-Y. et al., 2016. Comparison of cell behavior on pva/pva-gelatin electrospun nanofibers with random and aligned configuration. *Scientific Reports*, 6(1), p.37960. Available at: http://www.nature.com/articles/srep37960 [Accessed May 1, 2017].

Jayasinghe, S.N., 2013. Cell electrospinning: a novel tool for functionalising fi bres, scaff olds and membranes with living cells and other advanced materials for regenerative biology and medicine. *Analyst*, 138, pp.2215–2223. Available at: www.selectbio.com [Accessed March 20, 2017].

Jordá-Vilaplana, A. et al., 2014. Surface modification of polylactic acid (PLA) by air atmospheric plasma treatment. *European Polymer Journal*, 58, pp.23–33.

Ju, Y.M. et al., 2010. Bilayered scaffold for engineering cellularized blood vessels. *Biomaterials*,

31(15), pp.4313–21. Available at: http://www.ncbi.nlm.nih.gov/pubmed/20188414 [Accessed July 14, 2015].

Khan, F. et al., 2010. Strategies for cell manipulation and skeletal tissue engineering using high-throughput polymer blend formulation and microarray techniques. *Biomaterials*, 31, pp.2216–2228.

Kharaziha, M. et al., 2013. PGS:Gelatin nanofibrous scaffolds with tunable mechanical and structural properties for engineering cardiac tissues. *Biomaterials*, 34(27), pp.6355–6366.

Kim, S.-S. et al., 2003. Renal tissue reconstitution by the implantation of renal segments on biodegradable polymer scaffolds. *Biotechnology Letters*, 25, pp.1505–1508. Available at: http://link.springer.com/article/10.1023/A%3A1025490718221 [Accessed May 12, 2016].

Leong, M.F. et al., 2009. In vitro cell infiltration and in vivo cell infiltration and vascularization in a fibrous, highly porous poly(D,L-lactide) scaffold fabricated by cryogenic electrospinning technique. *Journal of biomedical materials research. Part A*, 91A(1), pp.231–40. Available at: http://www.ncbi.nlm.nih.gov/pubmed/18814222 [Accessed October 31, 2014].

Leong, M.F., Chan, W.Y. & Chian, K.S., 2013. Cryogenic electrospinning: proposed mechanism, process parameters and its use in engineering of bilayered tissue structures. *Nanomedicine (London, England)*, 8(4), pp.555–66. Available at: http://www.futuremedicine.com/doi/abs/10.2217/nnm.13.39%5Cnhttp://www.ncbi.nlm.nih.gov/pubmed/23560407.

Lowery, J.L., Datta, N. & Rutledge, G.C., 2010. Effect of fiber diameter, pore size and seeding method on growth of human dermal fibroblasts in electrospun poly(epsilon-caprolactone) fibrous mats. *Biomaterials*, 31(3), pp.491–504. Available at: http://www.sciencedirect.com/science/article/pii/S0142961209010242 [Accessed June 16, 2015].

Mahjour, S.B. et al., 2016. Improved cell infiltration of electrospun nanofiber mats for layered tissue

constructs. *Journal of Biomedical Materials Research Part A*, 104(6), pp.1479–1488. Available at: http://doi.wiley.com/10.1002/jbm.a.35676 [Accessed July 29, 2016].

Martins, A. et al., 2009. Surface modification of electrospun polycaprolactone nanofiber meshes by plasma treatment to enhance biological performance. *Small (Weinheim an der Bergstrasse, Germany)*, 5(10), pp.1195–206. Available at: http://www.ncbi.nlm.nih.gov/pubmed/19242938 [Accessed February 4, 2016].

McCullen, S.D. et al., 2012. Anisotropic fibrous scaffolds for articular cartilage regeneration. *Tissue engineering. Part A*, 18(19–20), pp.2073–83. Available at: http://www.pubmedcentral.nih.gov/articlerender.fcgi?artid=3463280&tool=pmcentrez&rendertype=abstract [Accessed December 26, 2014].

Moon, K.H. et al., 2016. Kidney diseases and tissue engineering. *Methods*, 99, pp.112–119. Available at: http://www.sciencedirect.com/science/article/pii/S1046202315300086 [Accessed April 12, 2017].

Mouras, R. et al., 2013. Multimodal, label-free nonlinear optical imaging for applications in biology and biomedical science. *Journal of Raman Spectroscopy*, 44(10), pp.1373–1378. Available at: http://doi.wiley.com/10.1002/jrs.4305 [Accessed August 5, 2016].

Nakayama, K.H. et al., 2010. Decellularized rhesus monkey kidney as a three-dimensional scaffold for renal tissue engineering. *Tissue engineering. Part A*, 16(7), pp.2207–16. Available at: http://www.pubmedcentral.nih.gov/articlerender.fcgi?artid=2947947&tool=pmcentrez&rendertype=abstract [Accessed November 3, 2014].

NHS Blood and Transplant, 2015. *Organ donation and transplantation Activity Report 2014-2015*, Available at: http://www.odt.nhs.uk/uk-transplant-registry/organ-specific-reports/.

NHS Kidney care, 2010. *Kidney Disease: Key Facts and Figures*,

NHS Organ Donation, 2014. *Activity Report 2013-2014*, Available at:

https://www.organdonation.nhs.uk/statistics/transplant_activity_report/current_activity_reports/ukt/kidney_activity.pdf.

O'Brien, F.J., 2011. Biomaterials & scaffolds for tissue engineering. *Materials Today*, 14(3), pp.88–95.

Peloso, A. et al., 2016. Extracellular matrix scaffolds as a platform for kidney regeneration. *European Journal of Pharmacology*. Available at: http://linkinghub.elsevier.com/retrieve/pii/S0014299916304770.

Petrigliano, F.A. et al., 2014. In Vivo Evaluation of Electrospun Polycaprolactone Graft for Anterior Cruciate Ligament Engineering. *Tissue Engineering Part A*, 21(March 2016), p.150127064142004. Available at: http://online.liebertpub.com/doi/full/10.1089/ten.tea.2013.0482.

Pham, Q.P., Sharma, U. & Mikos, A.G., 2006a. Electrospinning of polymeric nanofibers for tissue engineering applications: a review. *Tissue engineering*, 12(5), pp.1197–211. Available at: http://www.ncbi.nlm.nih.gov/pubmed/16771634.

Pham, Q.P., Sharma, U. & Mikos, A.G., 2006b. Electrospun poly(epsilon-caprolactone) microfiber and multilayer nanofiber/microfiber scaffolds: characterization of scaffolds and measurement of cellular infiltration. *Biomacromolecules*, 7(10), pp.2796–805. Available at: http://www.ncbi.nlm.nih.gov/pubmed/17025355.

Phipps, M.C. et al., 2012. Increasing the pore sizes of bone-mimetic electrospun scaffolds comprised of polycaprolactone, collagen I and hydroxyapatite to enhance cell infiltration. *Biomaterials*, 33(2), pp.524–34. Available at: http://www.sciencedirect.com/science/article/pii/S0142961211011720 [Accessed November 12, 2014].

Pu, J. et al., 2014. Electrospun bilayer fibrous scaffolds for enhanced cell infiltration and vascularization in vivo. *Acta biomaterialia*. Available at:

http://www.sciencedirect.com/science/article/pii/S174270611400508X [Accessed December 5, 2014].

Remuzzi, A. et al., 2017. Experimental Evaluation of Kidney Regeneration by Organ Scaffold Recellularization. *Scientific Reports*, 7(March 2016), p.43502. Available at: http://www.nature.com/articles/srep43502.

Saha, K. et al., 2007. Designing synthetic materials to control stem cell phenotype. *Current Opinion in Chemical Biology*, 11(4), pp.381–387.

Schutgens, F., Verhaar, M.C. & Rookmaaker, M.B., 2016. Pluripotent stem cell-derived kidney organoids: an in vivo-like in vitro technology. *European Journal of Pharmacology*, pp.1–9. Available at: http://linkinghub.elsevier.com/retrieve/pii/S0014299916304289.

Shah, S. et al., 2014. Guiding Stem Cell Differentiation into Oligodendrocytes Using Graphene-Nanofiber Hybrid Scaffolds. *Advanced Materials*, 26(22), pp.3673–3680. Available at: http://doi.wiley.com/10.1002/adma.201400523 [Accessed August 5, 2016].

Sill, T.J. & von Recum, H.A., 2008. Electrospinning: applications in drug delivery and tissue engineering. *Biomaterials*, 29(13), pp.1989–2006. Available at: http://www.sciencedirect.com/science/article/pii/S0142961208000203 [Accessed July 11, 2014].

Simonet, M. et al., 2007. Ultraporous 3D polymer meshes by low-temperature electrospinning: Use of ice crystals as a removable void template. *Polymer Engineering & Science*, 47(12), pp.2020–2026. Available at: http://doi.wiley.com/10.1002/pen.20914 [Accessed July 29, 2016].

Slater, S. et al., 2011. An In Vitro Model of the Glomerular Capillary Wall Using Electrospun Collagen Nanofibres in a Bioartificial Composite Basement Membrane. *PLoS ONE*, 6(6), p.e20802. Available at: http://linkhttp//journals.plos.org/plosone/article?id=10.1371/journal.pone.0020802.

Song, J.J. et al., 2013. Regeneration and experimental orthotopic transplantation of a bioengineered

kidney. *Nature medicine*, 19(5), pp.646–51. Available at: http://dx.doi.org/10.1038/nm.3154 [Accessed July 11, 2014].

Stalder, A.F. et al., 2006. A snake-based approach to accurate determination of both contact points and contact angles. *Colloids and Surfaces A: Physicochemical and Engineering Aspects*, 286(1), pp.92–103. Available at: http://www.sciencedirect.com/science/article/pii/S0927775706002214 [Accessed April 5, 2017].

Steele, J.A.M. et al., 2014. Combinatorial scaffold morphologies for zonal articular cartilage engineering. *Acta Biomaterialia*, 10(5), pp.2065–2075. Available at: http://dx.doi.org/10.1016/j.actbio.2013.12.030.

Straube, T. et al., 2011. Changes in the expression and subcellular distribution of galectin-3 in clear cell renal cell carcinoma. *Journal of experimental & clinical cancer research : CR*, 30(1), p.89. Available at: http://www.ncbi.nlm.nih.gov/pubmed/21958686 [Accessed August 4, 2016].

Suntornnond, R., An, J. & Kai Chua, C., 2016. Effect of gas plasma on polycaprolactone (PCL) membrane wettability and collagen type I immobilized for enhancing cell proliferation. *Materials Letters*, 171, pp.293–296. Available at: http://ac.els-cdn.com/S0167577X16302233/1-s2.0-S0167577X16302233-main.pdf?_tid=aeb071f4-25e0-11e7-9665-00000aab0f27&acdnat=1492703439_28ee111d9144153d35fcfdf27e708aa9 [Accessed April 20, 2017].

Taguchi, A. et al., 2014. Redefining the in vivo origin of metanephric nephron progenitors enables generation of complex kidney structures from pluripotent stem cells. *Cell stem cell*, 14(1), pp.53–67. Available at: http://www.ncbi.nlm.nih.gov/pubmed/24332837 [Accessed November 30, 2015].

Takasato, M. et al., 2014. Directing human embryonic stem cell differentiation towards a renal lineage generates a self-organizing kidney. *Nature cell biology*, 16(1), pp.118–26. Available at: http://dx.doi.org/10.1038/ncb2894 [Accessed June 7, 2015].

Takasato, M. et al., 2015. Kidney organoids from human iPS cells contain multiple lineages and model human nephrogenesis. *Nature*, 526(7574), pp.564–568. Available at: http://dx.doi.org/10.1038/nature15695 [Accessed October 9, 2015].

Townsend-Nicholson, A. & Jayasinghe, S.N., 2006. Cell Electrospinning: a Unique Biotechnique for Encapsulating Living Organisms for Generating Active Biological Microthreads/Scaffolds. *Biomacromolecules*, 7(12), pp.3364–3369. Available at: http://pubs.acs.org/doi/abs/10.1021/bm060649h [Accessed March 20, 2017].

Uzarski, J.S. et al., 2014. New strategies in kidney regeneration and tissue engineering. *Current opinion in nephrology and hypertension*, 23(4), pp.399–405. Available at: http://www.ncbi.nlm.nih.gov/pubmed/24848937 [Accessed September 23, 2014].

Waanders, F. et al., 2010. Kidney injury molecule-1 in renal disease. *The Journal of Pathology*, 220(1), pp.7–16. Available at: http://doi.wiley.com/10.1002/path.2642 [Accessed April 27, 2017].

Wang, J. et al., 2012. The effects of electrospun TSF nanofiber diameter and alignment on neuronal differentiation of human embryonic stem cells. *Journal of biomedical materials research. Part A*, 100A, pp.632–45.

Wang, Z. et al., 2014. The effect of thick fibers and large pores of electrospun poly(ε-caprolactone) vascular grafts on macrophage polarization and arterial regeneration. *Biomaterials*, 35(22), pp.5700–5710.

Wise, S.G. et al., 2011. A multilayered synthetic human elastin/polycaprolactone hybrid vascular graft with tailored mechanical properties. *Acta Biomaterialia*, 7(1), pp.295–303.

Wong, S.-C., Baji, A. & Leng, S., 2008. Effect of fiber diameter on tensile properties of electrospun poly(ε-caprolactone). *Polymer*, 49(21), pp.4713–4722.

Woodruff, M.A. & Hutmacher, D.W., 2010. The return of a forgotten polymer - Polycaprolactone in

the 21st century. *Progress in Polymer Science (Oxford)*, 35(10), pp.1217–1256.

Xia, Y. et al., 2013. Directed differentiation of human pluripotent cells to ureteric bud kidney progenitor-like cells. *Nature cell biology*, 15(12), pp.1507–15. Available at: http://dx.doi.org/10.1038/ncb2872 [Accessed October 29, 2014].

Xia, Y. et al., 2014. The generation of kidney organoids by differentiation of human pluripotent cells to ureteric bud progenitor–like cells. *Nature Protocols*, 9(11), pp.2693–2704. Available at: http://www.nature.com/doifinder/10.1038/nprot.2014.182 [Accessed October 24, 2014].

Xinaris, C. et al., 2012. In vivo maturation of functional renal organoids formed from embryonic cell suspensions. *Journal of the American Society of Nephrology : JASN*, 23(11), pp.1857–68. Available at: http://www.pubmedcentral.nih.gov/articlerender.fcgi?artid=3482737&tool=pmcentrez&rendertype=abstract [Accessed May 12, 2016].

Yan, D. et al., 2013. Plasma treatment of electrospun PCL random nanofiber meshes (NFMs) for biological property improvement. *Journal of Biomedical Materials Research Part A*, 101A(4), pp.963–972. Available at: http://doi.wiley.com/10.1002/jbm.a.34398 [Accessed April 20, 2017].

Yan, J. et al., 2012. Effect of fiber alignment in electrospun scaffolds on keratocytes and corneal epithelial cells behavior. *Journal of biomedical materials research. Part A*, 100(2), pp.527–35. Available at: http://onlinelibrary.wiley.com/doi/10.1002/jbm.a.33301/full [Accessed April 6, 2016].

Yu, Y.L. et al., 2014. Decellularized kidney scaffold-mediated renal regeneration. *Biomaterials*, 35(25), pp.6822–8. Available at: http://www.sciencedirect.com/science/article/pii/S0142961214004724 [Accessed October 23, 2014].

Yuan, Y. & Lee, T.R., 2013. Contact Angle and Wetting Properties. In *Surface Science Techniques*. Springer Berlin Heidelberg, pp. 3–34. Available at: http://link.springer.com/10.1007/978-3-642-

34243-1_1 [Accessed April 5, 2017].